A Soft Pressure Sensor Skin for Hand and Wrist Orthoses

Xinyang Tan[1], Liang He[1], Jiangang Cao[2], Wei Chen[2] and Thrishantha Nanayakkara[1]

***Abstract*—Side effects caused by excessive contact pressure such as discomfort and pressure sores are commonly complained by patients wearing orthoses. These problems leading to low patient compliance decrease the effectiveness of the device. To mitigate side effects, this study describes the design and fabrication of a soft sensor skin with strategically placed 12 sensor units for static contact pressure measurement beneath a hand and wrist orthosis. A Finite Element Model was built to simulate the pressure on the hand of a subject and sensor specifications were obtained from the result to guide the design. By testing the fabricated soft sensor skin on the subject, contact pressure between 0.012 MPa and 0.046 MPa was detected, revealing the maximum pressure at the thumb metacarpophalangeal joint which was the same location of the highest pressure of simulation. In this paper, a new fabrication method combining etching and multi-material additive manufacture was introduced to produce multiple sensor units as a whole. Furthermore, a novel fish-scale structure as the connection among sensors was introduced to stabilize sensor units and reinforce the soft skin. Experimental analysis reported that the sensor signal is repeatable, and the fish-scale structure facilitates baseline resuming of sensor signal during relaxation.**

***Index Terms*—Soft Sensors and Actuators; Force and Tactile Sensing; Human Factors and Human-in-the-Loop**

I. Introduction

HAND and wrist (h&w) orthoses have been commonly used in clinics to facilitate recovery of hand injuries [1], manage pain and prevent muscular disorders of chronic diseases such as Carpal Tunnel Syndrome [2] and stroke [3]. A h&w orthosis is usually customized with Low Temperature Thermoplastic (LTT) [4] to fit to hands of patients, aiming to stabilize or limit the range of motion of affected joints and remain or assist mobility of unaffected joints [1].

Patients are usually encouraged to wear h&w orthoses as often as possible for a long period, for instance, 4 to 6 weeks for tendon injuries [5] and maybe years for post stroke patients [3]. Discomfort has been considered one of the main reasons of low patient compliance which leads to decreased effectiveness of h&w orthoses [6] and pressure sores are commonly seen due to prolonged pressure [7]. Challenges have been found in clinics to minimize excessive pressure. First, discomfort caused by excessive pressure is normally expressed subjectively by patients. However, due to the unknown pressure distribution beneath orthoses, desired adjustments to mitigate discomfort cannot be efficiently achieved. Second, the sensation of discomfort or pain exacerbates with time, as tissue damages progressively worsen [8]. Thus, patients may not feel the discomfort and pain until after they have left the clinics, leaving the sensation unreported. Softer materials [9] and paddings [1] were used trying to minimize contact pressure. However, decreasing the rigidity of the material could not efficiently reduce side effects and may also decrease the effectiveness of orthoses [9], as the soft material was not accurately added at the key locations.

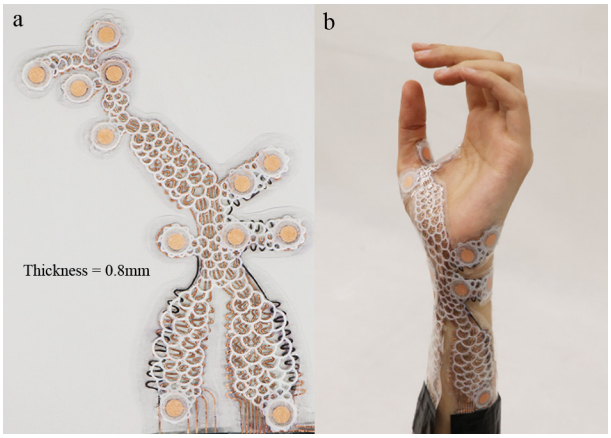

Fig. 1. The soft sensor skin with strategically placed pressure sensors in a novel non-homogeneous stretchable layered structure.

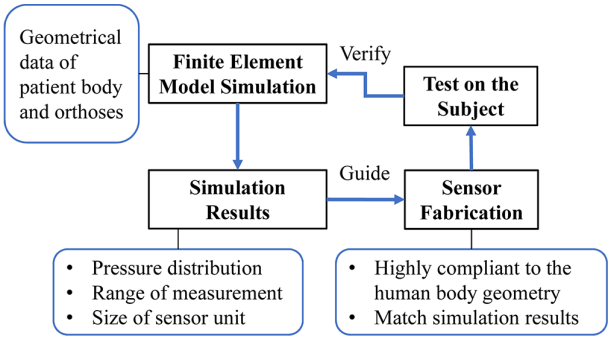

Fig. 2. Sensor development with a patient-involved approach.

Manuscript received: September, 10, 2019; Revised December, 15, 2019; Accepted January, 23, 2020.

This paper was recommended for publication by Editor Kyu-Jin Cho upon evaluation of the Associate Editor and Reviewers' comments. This work was partly supported by the Xuzhou Central Hospital, the China Scholarship Council and the UK Engineering and Physical Sciences Research Council (EPSRC) under MOTION Grant EP/N03211X/2. (Corresponding authors: Xinyang Tan and Wei Chen.)

[1]X. Tan, L. He and T. Nanayakkara are with the Dyson School of Design Engineering, Imperial College London, London SW7 2DB, UK xinyang.tan14@imperial.ac.uk

[2]J. Cao and W. Chen are with the Rehabilitation Department, Xuzhou Central Hospital, Xuzhou City, Jiangsu province 221009, China chenwei2339@163.com

Digital Object Identifier (DOI): see top of this page.

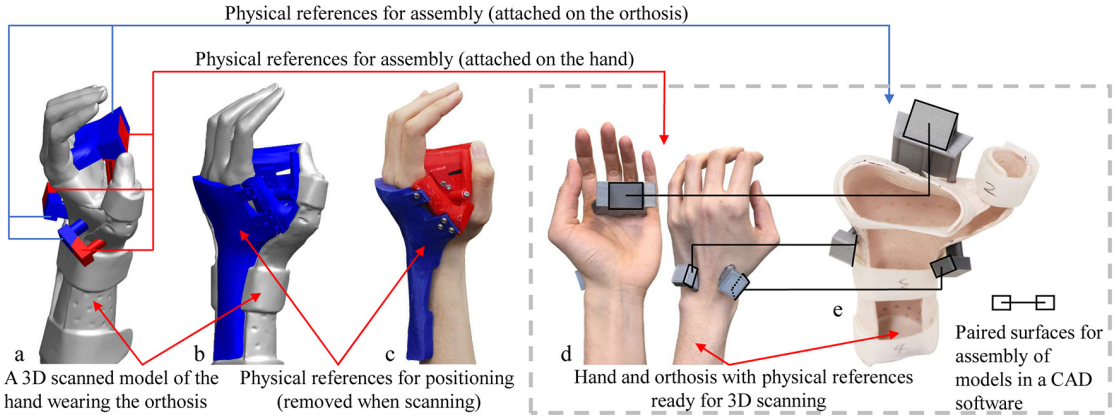

Fig. 3. Physical references for 3D scanning and model assembly. (a) Design of physical references for assembly (PRA). (b) Design of physical references for positioning (PRP). (c) 3D printed PRP placed on the hand to keep main joints angles the same as wearing the orthosis before scanning. (d) PRA attached on the hand with silicone tape. (e) PRA attached on the orthosis using super glue.

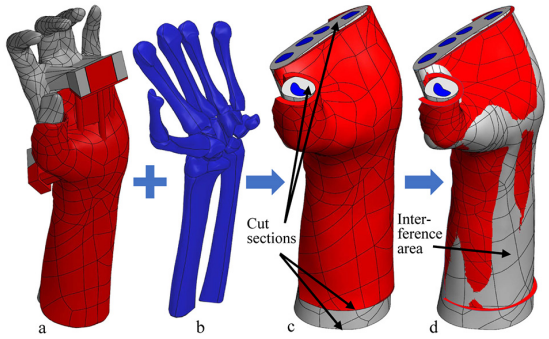

Fig. 4. Assembly and processing of 3D scanned models. (a) 3D scanned hand and orthosis models were assembled by matching paired surfaces. (b) A modified CAD model of hand bones was added to the assembly. (c) Physical references and extra parts were removed. Parallel cut sections were created. (d) Simplified the solid orthosis model into a surface model.

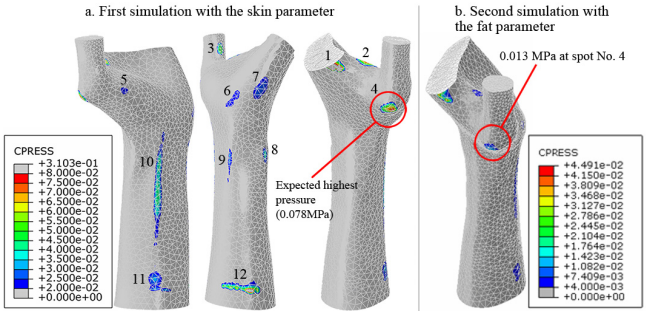

Fig. 5. The results of the two simulations showed the same distribution of contact pressure with different pressure magnitudes. The highest value was at the spot No. 4 and the spots No. 1 and 12 were not considered as higher pressure spots, which was explained in the section.

Therefore, a pressure sensitive orthosis is in need to allow therapists and patients to identify and monitor excessive pressure to enable the most efficient adjustment and minimize side effects. This paper presents a novel soft sensor skin (Fig. 1) that is highly compliant with human hands and orthoses.

Studies have been conducted to measure pressure on the hand skin to mitigate hazards during treatments or daily activities. Pressure distribution under a wrist orthosis for patients with Carpal Tunnel Syndrome at various wrist angles was measured in a study using a commercial capacitive sensor mat [2]. Contact force was also measured using separated resistive pressure sensor pads on key sensitive positions of a forearm for designing a h&w orthosis [10]. Moreover, contact pressure was measured in a study [11] to improve comfort of upper-limb prostheses. Apart from hands, skin contact pressure was also measured at the face [12] and the feet [13] in attempt to increase comfort or minimize risks of injuries. However, most studies used off-the-shelf sensors, which presented some difficulties. For instance, standardized sensors may not suit the particular measuring purpose, as the sensor shape does not conform to the complicated geometry of the human body. Also, their sensing units may not be placed in the desired distribution for capturing data from key points on the skin.

Many soft sensors with pressure measurement have been developed with optical [14], resistive [15], capacitive [16] and magnetic [17] techniques. According to a study revealing criteria of soft sensor development from the perspective of patients, wearable sensors need to be comfortable and compact [18]. However, most wearable soft sensors follow the one for all strategy rather taking users into consideration. Therefore, this study proposes a patient-involved sensor development approach shown in Fig. 2 to design and fabricate a soft sensor skin for patients wearing h&w orthoses. In order to clarify the approach, a Finite Element Model (FEM) of a customized orthosis worn by a healthy subject was established. Design specifications of the soft sensor skin were derived from results of simulations. A new fish-scale enhancement structure and a plating layer were embedded into the sensor, and their functional purposes were demonstrated in this paper. The rest of the paper is organized as follows: Section II explains the design and fabrication of the sensor skin. The results of characterization of the sensor and the test on a subject wearing the customized orthosis are presented in section III. Opportunities for future research are elaborated in section IV. Finally, section V provides concluding remarks on the design and results.

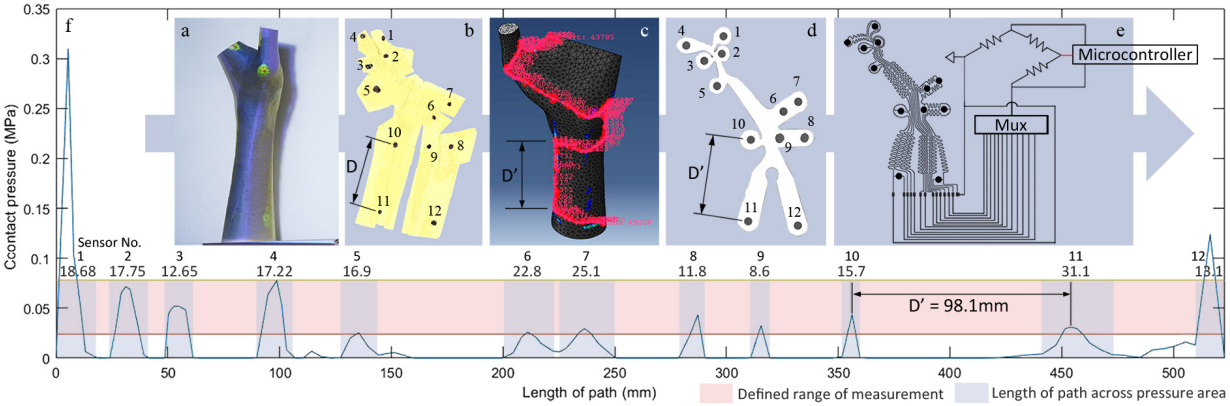

Fig. 6. The process of generating the 2D pressure distribution pattern. (a) Projected Abaqus result on a 3D printed hand model which was covered with masking tape. (b) Pressure spots were marked on the tape and it was flattened to generate a 2D pattern with rough distances between spots, e.g. rough distance D between spot No. 10 and 11. (c) In Abaqus, drew a path on the surface of the model to link centers of pressure spots. It created the true distance between any two consecutive spots, e.g. true distance D′ between spot No. 10 and 11. (d) Generated the final 2D pressure distribution pattern by correcting distances (e.g. correct D to D′). (e) Designed circuit based on the pattern. (f) The path was plotted with contact pressure along with it, showing 12 pressure spots as peaks within the range of measurement and the length of path across each pressure area.

II. Methods

A. FEA of an Orthosis Worn on Hand

In order to understand the geometry of the contact area beneath a customized h&w orthosis, a FEM was built to simulate the contact pressure on the hand of a healthy male adult. The orthosis is the most common type made of the LTT material by a professional hand therapist. The subject was informed of the experiment procedure approved by the Xuzhou Central Hospital Biomedical Research Ethics Committee and the Imperial College Research Ethics Committee.

The hand of the subject in the position of wearing the orthosis was 3D scanned. Since it is difficult to keep all joint angles the same as stabilized by the orthosis, physical references were designed in a CAD software and 3D printed, based on a 3D scanned model of the hand wearing the orthosis (Fig. 3a, b). Before scanning, the orthosis was worn on the hand of the subject. Physical references for assembly (PRA) were placed on both the hand and the orthosis to find their corresponding locations according to the arrangement in Fig. 3a and the locations were marked manually. PRA were attached on the orthosis using super glue (see Fig. 3e). Then, after taking off the orthosis, the physical references for positioning (PRP) as shown in Fig. 3c were placed on the hand to convert main joints to desired angles. The subject was asked to keep the hand steady and the PRP were removed. According to markings, PRA were attached on the hand as shown in Fig. 3d using silicone tapes. The hand with PRA was scanned using a handhold 3D scanner (Artec EVA-M 3D scanner, Artec 3D). The orthosis with PRA was also scanned using another 3D scanner (Artec Space Spider, Artec 3D). Small holes of the orthosis were filled with clay in advance in order to simplify the simulation, as holes are designed for breathability, barely affecting contact pressure. As seen from Fig. 4a, the hand and the orthosis models were assembled together in a CAD software by matching paired surfaces of physical references (Fig. 3e), which were cut off afterwards. A CAD model of hand bones of a healthy male adult was provided by the hospital based on the computerized tomography (CT) data (Fig. 4b). The bones model was modified anatomically according to the hand of the subject in terms of size, joint angles and key positions of each bone in order to be embedded into the 3D scanned hand. The assembly model of the hand, the bones and the orthosis is shown in Fig. 4c. Cut sections were created by cutting unattached edges and parts at the distal and the proximal ends of the orthosis, the hand and bones, so they could be assembled accurately in Abaqus (Abaqus 2018, Dassault Systemes, France) by mating the cut sections. The inside surface of the orthosis was created instead of a solid part to simplify the Finite Element Analysis (FEA) (Fig. 4d).

Two simulations were conducted with parameters of skin and fat assigned respectively to the soft tissue of the hand model. As skin is more rigid than fat, an approximate range of contact pressure provided by the orthosis can be achieved. The Young's modulus of skin (0.177 MPa) [19] and fat (0.034 MPa) [20] were obtained from literatures. Since the soft tissue is almost incompressible, its Poisson's ratio was set as 0.45 [21]. The Young's modulus of 15 GPa and the Poisson's ratio of 0.3 were set for bones [22]. As mechanical properties of the LTT material were not available from the manufacturer, a tensile strength test was conducted on five LTT samples following the ISO 527-1993 standard using the MZ-4000D1 tensile strength test machine (MingZhu Instruments Ltd., China). The average modulus of elasticity in tension is 393.3 MPa. Its Poisson's ratio was set as 0.34 from the literature using a similar LTT material [23].

According to the FEA result shown in Fig. 5a - the first simulation using the skin parameter, 12 pressure area scattered over the hand surface with values higher than 0.02 MPa which may bring discomfort [24] were identified as the measurement area with spot number from 1 to 12. The highest contact pressure was 0.31 MPa at the spot No. 1. However, it was not considered as the highest, as it was caused by the cut section without boundary conditions, leading to an abnormal deformation. Another area at the proximal end of the ulnar side of the orthosis (spot No. 12) with the second highest pressure (0.12 MPa) was not considered as the highest pressure either,

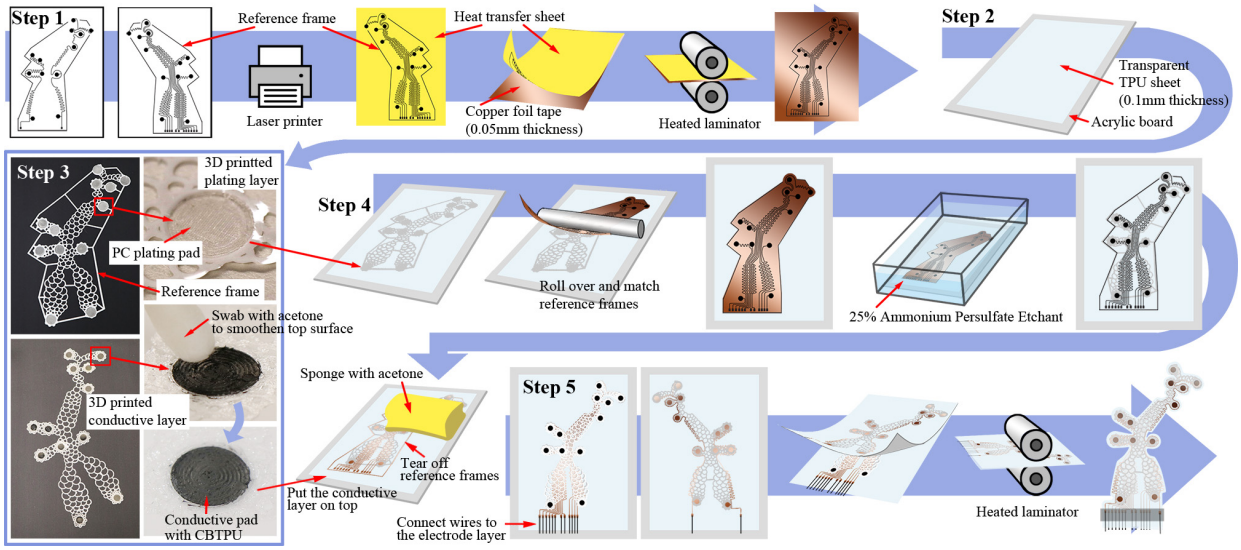

Fig. 7. Fabrication process of the soft sensor skin.

since it resulted from the boundary conditions of the orthosis and the forearm. Therefore, the third highest pressure point at the thumb metacarpophalangeal (MCP) joint (spot No.4) was considered as the maximum pressure with 0.078 MPa. From the second simulation using the fat parameter in Fig. 5b, only spot No.4 was revealed with pressure higher than 0.01 MPa. The two simulations showed the same pressure distribution with different pressure magnitudes. Thus, the distribution of 12 spots was employed to extract the placement of sensor units of the soft sensor skin.

B. Generate the 2D Pressure Distribution Pattern

As the FEA result was presented on a 3D model, it was a challenge to convert the pressure distribution in a complex 3D space into a flat 2D pattern which could fit around the surface of the 3D model. A solution was proposed as follows using a projector and a path plot in Abaqus [25]. The Abaqus result was projected on a 3D printed full-scale hand model of the subject as shown in Fig. 6a. A layer of masking tape was evenly covered over the pressure area of the 3D printed hand. Locations of pressure spots were marked manually on the masking tape according to the projection. Then, the tape was peeled off from the hand model and flattened to generate a rough 2D pressure distribution pattern (Fig. 6b). A path was drawn on the surface of the hand model in Abaqus connecting all pressure spots (Fig. 6c). The path was plotted in Fig. 6f with contact pressure along with it, displaying the true distance of curved linkages between any two consecutive pressure spots. The rough 2D pressure distribution pattern was modified by correcting distances between pressure spots using the length of path in Fig. 6f to achieve a more accurate distribution pattern as shown in Fig. 6d. If each contact area is considered as a circular spot, the diameter can be derived from the length of path across each pressure area (Fig. 6f). The minimum dimension of 8.6 mm (approximately 9 mm) was selected as the diameter of the circular sensor unit. Cables were designed within the pattern contour and externally connected to a

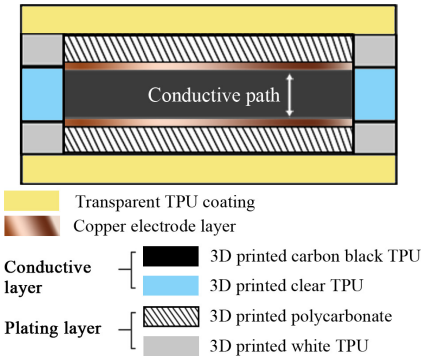

Fig. 8. Sensor unit configuration. The carbon black TPU acts as the pressure sensitive material in terms of change of resistance.

Wheatstone Bridge through a multiplexer. Data was collected by a microcontroller (Arduino Mega 2560 Rev3) as shown in Fig. 6e.

Therefore, design specifications of the soft sensor skin were obtained through the FEA process. Specifically, a soft sensor skin consisting of 12 circular sensor units (⌀9 mm) placed in the 2D pressure distribution pattern should be fabricated, with measurement range covering the span from 0.02 MPa to 0.078 MPa.

C. Design and Fabrication of the Soft Sensor Skin

Five steps are shown in Fig. 7 regarding fabrication of the soft sensor skin with seven layers (Fig. 8), including two transparent thermoplastic polyurethane (TPU) coatings, two 3D printed polycarbonate (PC) and TPU plating layers, two copper electrode layers and one 3D printed carbon black TPU (CBTPU) and clear TPU conductive layer with about 0.8 mm thickness in total. The sensor resistance decreases when pressure is loaded as the conductive path of the CBTPU is shortened.

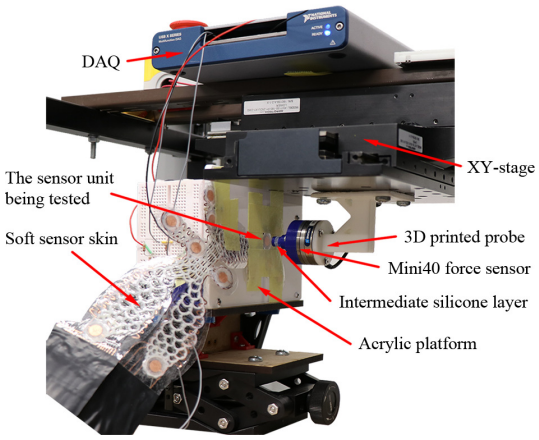

Fig. 9. Experiment setup for sensor characterization.

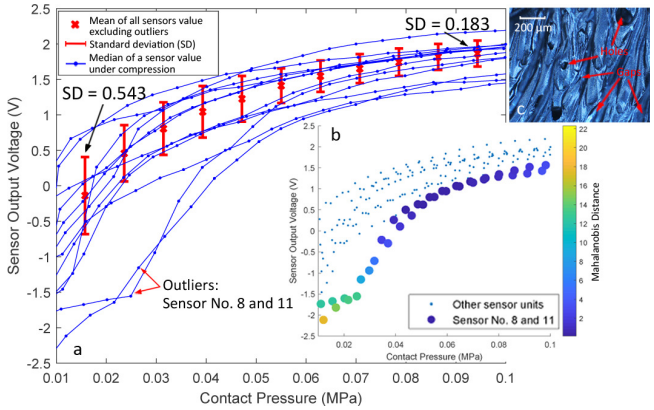

Fig. 10. (a) Pressure response of 12 sensor units. Each sensor unit was pressed by the probe with contact pressure from 0.01 MPa to 0.1 MPa (5 minutes compression and 1 minute relaxation). The figure shows correlation between the median of each sensor value and the contact pressure during compression. (b) Two outliers were found using the Mahalanobis distance. (c) Micro-structure of a conductive pad, figure captured using an optical microscope (ZEISS Axio Lab.A1, Zeiss, Germany).

1) Step 1. Pattern Preparation: Reference frames for easy locating at the later step 4 were added to the two half patterns which were divided from the 2D pressure distribution pattern. The pattern was printed on a heat transfer sheet using a laser printer (HP LaserJet MFP E87650dn Plus) and it was placed on a 0.05 mm thickness copper foil tape which has acrylic adhesive on the back. The pattern ink was transferred to the copper foil when the two overlapped pieces went through a heated laminator at about 135°C.

2) Step 2. TPU Coatings: A transparent TPU sheet with 0.1 mm thickness was placed on an acrylic board. Air bubbles between the TPU sheet and the board was manually pushed out through edges until the sheet was attached evenly.

3) Step 3. Multi-material printed plating and conductive layers: The plating layer and the conductive layer were 3D printed using a 3D printer (Ultimaker 3 extended, Ultimaker B.V.). The plating layer was multi-material printed in the thinnest available thickness (0.15 mm), specifically with material PC (Ultimaker PC filament) printed as the plating pads (14 mm diameter) and white TPU (Ultimaker TPU filament) printed as the connection. A reference frame was included in the plating layer for locating at the next step 4. The ironing function of the 3D printer is recommended as it smoothens the top surface of the PC plating pads. To build the conductive layer, a TPU filament containing carbon black (Palmiga - PI-ETPU 95-250, Palmiga Innovation AB, Sweden) was used to print conductive pads with the fish-scale enhancement structure around them which was printed with clear TPU filament (Orbi-Tech GmbH, Germany). Its thickness was set as 0.2 mm as the most qualified and the thinnest available thickness of the 3D printer. Acetone was swabbed on conductive pads as it melts and smoothens the top surface. Functional purposes of the plating layer and the fish-scale structure have been explained in section III.

4) Step 4. Etching to make the copper electrode layer: The plating layer was placed on top of the transparent TPU coating and the copper foil tape with the ink of pattern was adhered on top of it by matching reference frames. A rod was used to roll over the copper foil tape to enable full adhesion. Then, the acrylic board with attached layers was sunk in the 25% Ammonium Persulfate (APS) solution which was a mixture of 75g solid APS and 300g distilled water. Copper that was not covered by the transferred ink was corroded by the solution and only copper under the pattern remained. After all uncovered copper was etched, the board was taken off from the etchant and the solution residual was washed out by water, afterwards, wiping dry the layers. The transferred ink especially at electrode pads was gently wiped off using a sponge with pure acetone.

5) Step 5. Assembly of all layers: The above steps were repeated to complete another half of the sensor skin. Wires were connected to the copper electrode layer using copper foil tapes. The 3D printed conductive layer was placed on one of the copper electrode layers by matching centers of electrode pads and conductive pads. Both half skins were peeled off from acrylic boards and combined together by matching centers of sensor units. They were sealed together using a heated laminator with temperate of 135°C. Extra material of the transparent TPU coating was cut off along the contour of the pattern. A soft sensor skin was completed (Fig. 1a).

D. Experiment Setup

The experiment setup is shown in Fig. 9. One of the 12 sensor units was attached on the acrylic platform with double-sided tape. A 3D printed rigid probe (30 mm length) with a flat tip (⌀9 mm) was used to apply pressure directly on the sensor. A silicone layer (3 mm thickness, Eco-flex 0030, Smooth-on, USA) was placed in the middle of the probe to prevent over-loaded force. The probe connected to the ATI Mini40-E Force/Torque sensor (SI-40-2, ATI Industrial Automation, USA) was installed on an ANT130 XY-stage (Aerotech Inc., accuracy of 2.5 μm) which was used to control the position of the probe. At the beginning of each compression, the tip was barely touching the surface of a sensor unit, and then it moved towards the sensor for a pre-defined distance and applied pressure for a period of time. Afterwards, it moved

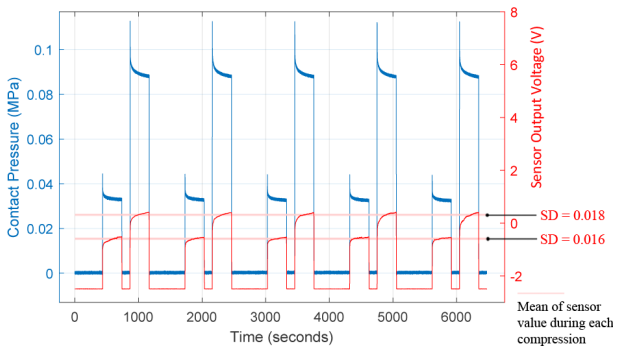

Fig. 11. The repeatability test was conducted on senor unit No.4 with contact pressures (blue line) of 0.033 MPa and 0.089 MPa respectively. In each trial, two contact pressures were given for 5 minutes with a 2 minutes relaxation in-between and 5 trials of the test were conducted with 550 seconds in-between. For each contact pressure, the standard deviation (SD) of means of sensor outputs (pink line) across 5 trails is reported.

back to its no contact position for sensor relaxation. The sensor voltage outputs were collected using the National Instrument DAQ (USB-6341) and Labview 2018 during characterization test.

III. RESULTS

A. Pressure response of the soft sensor skin

The pressure response of the soft sensor skin was evaluated. Fig. 10a shows the test result of applied pressure from 0.01 MPa to 0.1 MPa. In each step of compression, the probe made an incremental indentation of 0.1 mm on the sensor unit. For instance, it moved towards the sensor from the no contact position for 0.1 mm, 0.2 mm and 0.3 mm at the 1st, the 2nd, and the 3rd time of compression respectively. The median of sensor outputs and the contact pressure obtained from the Mini40 force sensor within each stabilized compression period was calculated and their correlation was reported. Two sensor units (No. 8 and 11) were found as outliers using Mahalanobis distance and were likely due to unclear fabrication errors (Fig. 10b). At the same contact pressure, voltages from different sensors tend to be closer, as the standard deviation (excluding the outliers) decreases from 0.543 at 0.016 MPa to 0.183 at 0.094 MPa. This result may be due to the unevenly distributed voids or gaps of the conductive elastomer generated during 3D printing (Fig. 10c). When the same pressure was applied, deformations of conductive pads were slightly different, as the Young's modulus were different due to variance of porosity [26]. However, when contact pressure increased, voids were squeezed and the micro-structure of different conductive pads became similar, leading to smaller standard deviation. Further investigation on the micro-structure will be conducted to clarify this phenomenon. Although, standard deviation seems large, 10 out of 12 sensor units (83.3%) showed identical pressure response, indicating the reliability of the fabrication process. Since each sensor unit was calibrated individually, it did not influence the function of the soft sensor skin. Additionally, data were fitted to third-degree polynomials using the Least-squares fitting method to derive the calibration model that was used for test on human hand in III-E.

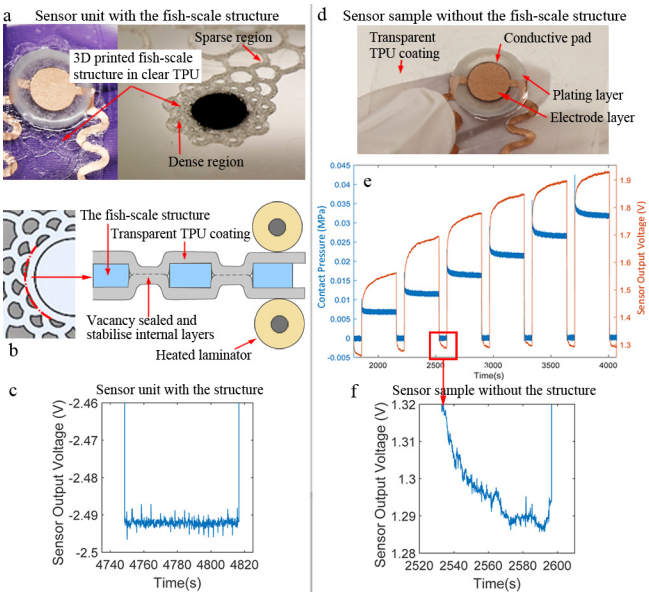

Fig. 12. Comparison between sensors with and without the fish-scale structure. (a) Sensor unit with the fish-scale enhancement structure. (b) Section view of the fish-scale structure sealed between TPU coatings. (c) Data of a sensor unit with the fish-scale structure during 1 minute relaxation. (d) A sample sensor without the fish-scale structure. (e) The sample was pressed by the probe from 0 MPa to 0.08 MPa with 18 steps (5 minutes compression for each step and 1 minute relaxation in-between). A period (from 30 to 68 minute) with relatively more stable sample data is shown. (f) Zoomed in data of the sensor sample without the fish-scale structure during 1 minute relaxation. Clear difference shown between c and f due to the effect of the fish-scale structure.

B. Sensor Repeatability

In order to evaluate repeatability of the sensor, an experiment was performed as shown in Fig. 11. The standard deviations of means of the soft sensor value at each contact pressure across five trials were reported, specifically 0.016 at 0.033 MPa and 0.018 at 0.089 MPa. The result shows that the sensor output is repeatable. Additionally, due to the stress relaxation of the silicone layer in the probe, spikes at the beginning of the signal followed with a decrease occur at the contact pressure measured by the Mini40 sensor (Fig. 11). Moreover, it should be noted that although a slight increase can be observed in the soft sensor output after adding pressure, the output voltage shows a significant convergent trend over time, as the standard deviation of sensor values shown in Fig. 11 decreases from 0.045 between 880s and 930s to 0.012 between 980s and 1030s and continuously declines to 0.009 between 1080s and 1130s. Similar upward drifts have also been found in the literature [27] which clarified that the drift is caused by breaking of carbon chains in the conductive elastomer. Future study will be conducted to further investigate the drift and reduce it.

C. The fish-scale Structure of the Conductive Layer

Three functional purposes of the non-homogeneous fish-scale enhancement structure are demonstrated below: 1) It consists of a dense region which was designed to reinforce around the CBTPU (Fig. 12a), inhibiting stretching of the conductive pad. The clear TPU coating was heat-sealed through

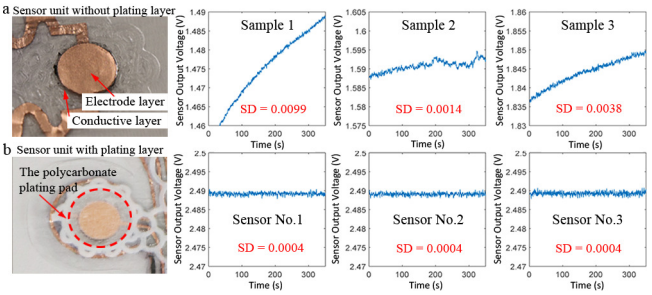

Fig. 13. Comparison of sensor units with and without the plating layer. Drift test at no loading for 350 seconds on (a) three sensor samples without the plating layer, and (b) three sensor units with the plating layer from the soft sensor skin (No. 1, 2 and 3). The Savitzky-Golay filter was applied for all data.

holes of the fish-scale structure surrounding the conductive pad (Fig. 12b) to prevent the pad from moving relative to the electrode. 2) When the applied force is withdrawn, the partly deformed elastic fish-scale structure around the pad facilitates the shape recovery of the deformed conductive pad, quickening signal restoring to the baseline, compared with a sensor sample without the fish-scale structure which is shown in Fig. 12d. The comparison during one minute relaxation was reported in Fig. 12c and f. It can be noted that, the sensor unit with the fish-scale structure has a faster response compared to that without the fish-scale structure during relaxation. 3) As the TPU coating is very soft and thin, the fish-scale structure aims to prevent over-stretching and tearing of the soft sensor skin. Meanwhile, it retains flexibility of the skin in the sparse region (Fig. 12a).

D. The Plating Layer

The functional purpose of the plating layer is to prevent signal drift at no loading. A drift test was conducted as shown in Fig. 13 with three sensor samples without the plating layer compared with three sensor units with the plating layer from the soft sensor skin. Signal drift was found in all sensor samples without the plating layer during a 350 seconds test at no-load condition and no drift was found from the three sensor units with the plating layer. Presumably, the plating pad printed with the PC material builds a relatively harder surface which supports the electrode pad and the conductive pad, enabling an even contact between the two layers and also preventing slight deformation of the conductive pad, therefore, reducing the drift. A micro level study will be conducted to clarify its function.

E. Test on the human hand

The test on the human hand was conducted as shown in Fig. 14 to evaluate the soft sensor skin worn by the subject. Data was collected from all sensor units when the soft sensor skin was attached for 28.5 minutes, and the orthosis was worn on top of it. Though the subject was asked to hold the hand steady, change of pressure was found in all sensor units due to inevitable movements. The data was biased to zero before analysis, as baselines of some pressure data were off-set from

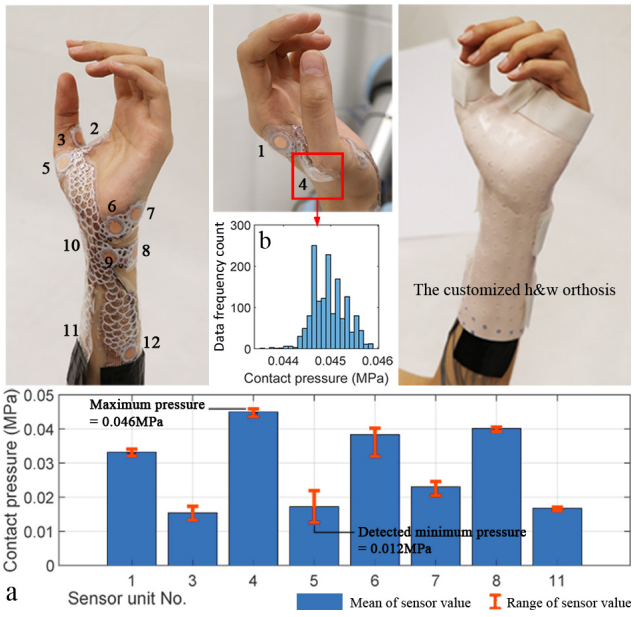

Fig. 14. Soft sensor skin was attached on the hand of the subject and the orthosis was worn on it for 28.5 minutes when collecting sensors value. 25.5 minutes of stabilized data from the 12 sensor units was selected. Pressure was detected in 8 out of 12 sensor units as shown in the figure. (a) Means and ranges of the 8 sensor outputs. (b) The histogram of data of the sensor unit No.4.

0 MPa due to initial deformation of bending. Contact pressure was detected in 8 out of 12 sensor units with a range from 0.012 MPa at sensor No. 5 to 0.046 MPa at sensor No. 4. It was expected that no contact pressure was measured from the other four sensor units (No. 2, 9, 10 and 12) likely due to too little pressure (lower than 0.01 MPa), as material properties at the four locations were closer to fat than skin. The four sensors at bony prominences (No. 1, 4, 6 and 8) all showed high magnitudes (over 0.03 MPa). The highest measurement was at the same location of the highest contact pressure of both FEA results (Fig. 5) and within the range of simulation from 0.013 MPa to 0.078 MPa. The second highest pressure (0.041 MPa) was measured by the sensor unit No. 8 at which the area presented the similar value (0.045 MPa) from the first simulation, indicating that the overall tissue parameter at this location is similar to skin. Maximum values measured at the spot No. 5 and 7 showed relatively high pressure over 0.02 MPa which may bring discomfort. However, since they do not locate at bony prominences, the two spots may be neglected by hand therapists during customization of orthoses. The application of the soft sensor skin could avoid this negligence.

IV. DISCUSSION

The main purpose of the FEA was to extract the distribution of pressure spots to guide the design of sensor placement rather having the absolute value at a specific spot, which was difficult to be simulated due to the complexity of human tissues. The discrepancy between simulated and experimental magnitudes were likely due to: (1) the difference between material parameters for the FEA and the actual material properties of hand tissues. For instance, the sensor value of

spot No. 4 was different from results of both simulations, as the soft tissue at the thumb joint was not pure fat or skin. The real material property may be within the range of parameters of the two simulations. (2) Though the bones model was modified anatomically based on the hand of the subject, differences between the model and real bones may affect the simulated magnitudes. (3) The geometrical difference between the real hand and the FEM may also slightly influence the result. Though 3D scanning with physical references was employed to achieve the hand model as accurately as possible, slight difference may exist due to inevitable motions during scanning and mesh creation during the FEA. Although the difference of magnitudes was found between the simulation and the measurement, the sensor placement was successfully derived from the simulation and the possible excessive pressure spots were in agreement.

Since the sensor skin was developed based on one subject, it cannot fit all sizes of human hands, though the soft sensor skin is stretchable due to elasticity of TPU. A future study will be conducted to create several 2D pressure distribution patterns through the proposed process on a group of subjects, covering major symptoms and common types of orthoses. Furthermore, the correlation between contact pressure value and feedback of patients regarding comfort will be disclosed to assist orthoses fabrication. Another future opportunity is to embed the soft sensor skins into orthoses. This will allow us to provide or release contact pressure, e.g. using jamming mechanisms [28], based on periodic sensor readings.

V. CONCLUSIONS

In this paper, a resistive soft sensor skin for static contact pressure measurement between a hand and an orthosis was developed. Following a patient-involved approach, a Finite Element Model was built to generate design specifications of the sensor to guide the fabrication. Multi-material 3D printing was used to fabricate 12 sensor units at once, comprising a novel fish-scale enhancement structure with dense and sparse regions. The fish-scale structure provides faster sensor response during relaxation, stabilizes sensor units against stretching and reinforces the skin. A 3D printed plating layer was also embedded in the sensor to reduce drift at no loading. The sensor test on the subject showed that the soft sensor skin is able to distinguish pressure differences and measure relatively high contact pressure on the hand. The soft sensor skin will be applied in the rehabilitation department to assist orthoses fabrication as hand therapists can directly customize orthoses on the sensor when patients are wearing it.

REFERENCES

[1] E. E. Fess and C. A. Philips, *Hand splinting: principles and methods*. Mosby Incorporated, 1987.

[2] Y. Cha, "Changes in the pressure distribution by wrist angle and hand position in a wrist splint," *Hand Surgery and Rehabilitation*, vol. 37, no. 1, pp. 38–42, 2018.

[3] A. Andringa, I. van de Port, and J.-W. Meijer, "Long-term use of a static hand-wrist orthosis in chronic stroke patients: a pilot study," *Stroke research and treatment*, vol. 2013, 2013.

[4] D. E. Breger-Lee and W. L. Buford Jr, "Properties of thermoplastic splinting materials," *Journal of Hand Therapy*, vol. 5, no. 4, pp. 202–211, 1992.

[5] T. Purcell, P. Eadie, S. Murugan, M. O'DONNELL, and M. Lawless, "Static splinting of extensor tendon repairs," *Journal of Hand Surgery*, vol. 25, no. 2, pp. 180–182, 2000.

[6] F. Sandford, N. Barlow, and J. Lewis, "A study to examine patient adherence to wearing 24-hour forearm thermoplastic splints after tendon repairs," *Journal of Hand Therapy*, vol. 21, no. 1, pp. 44–53, 2008.

[7] J. Buurke, J. Grady, J. De Vries, and C. T. Baten, "Usability of thenar eminence orthoses: report of a comparative study," *Clinical rehabilitation*, vol. 13, no. 4, pp. 288–294, 1999.

[8] I. Hoogendoorn, J. Reenalda, B. F. Koopman, and J. S. Rietman, "The effect of pressure and shear on tissue viability of human skin in relation to the development of pressure ulcers: a systematic review," *Journal of tissue viability*, vol. 26, no. 3, pp. 157–171, 2017.

[9] M. Hermann, T. Nilsen, C. S. Eriksen, B. Slatkowsky-Christensen, I. K. Haugen, and I. Kjeken, "Effects of a soft prefabricated thumb orthosis in carpometacarpal osteoarthritis," *Scandinavian journal of occupational therapy*, vol. 21, no. 1, pp. 31–39, 2014.

[10] W. Yan, M. Ding, B. Kong, X. Xi, and M. Zhou, "Lightweight splint design for individualized treatment of distal radius fracture," *Journal of medical systems*, vol. 43, no. 8, p. 284, 2019.

[11] J. Fu, H. Nguyen, D. W. Kim, C. Shallal, S. M. Cho, L. Osborn, and N. Thakor, "Dynamically mapping socket loading conditions during real time operation of an upper limb prosthesis," in *40th IEEE EMBC*, 2018, pp. 3930–3933.

[12] D. Dellweg *et al.*, "Determinants of skin contact pressure formation during non-invasive ventilation," *Journal of biomechanics*, vol. 43, no. 4, pp. 652–657, 2010.

[13] C. G. Tompkins and J. S. Sharp, "Dual optical force plate for time resolved measurement of forces and pressure distributions beneath shoes and feet," *Scientific reports*, vol. 9, no. 1, pp. 1–9, 2019.

[14] S. Sareh *et al.*, "Bio-inspired tactile sensor sleeve for surgical soft manipulators," in *IEEE ICRA*, 2014, pp. 1454–1459.

[15] T. Kim and Y.-L. Park, "A soft three-axis load cell using liquid-filled three-dimensional microchannels in a highly deformable elastomer," *IEEE Robotics and Automation Letters*, vol. 3, no. 2, pp. 881–887, 2018.

[16] P. Roberts, D. D. Damian, W. Shan, T. Lu, and C. Majidi, "Soft-matter capacitive sensor for measuring shear and pressure deformation," in *IEEE ICRA*, 2013, pp. 3529–3534.

[17] D. S. Chathuranga, Z. Wang, Y. Noh, T. Nanayakkara, and S. Hirai, "Magnetic and mechanical modeling of a soft three-axis force sensor," *IEEE Sensors Journal*, vol. 16, no. 13, pp. 5298–5307, 2016.

[18] J. H. Bergmann, V. Chandaria, and A. McGregor, "Wearable and implantable sensors: the patient's perspective," *Sensors*, vol. 12, no. 12, pp. 16 695–16 709, 2012.

[19] A. Yu, K. L. Yick, S. P. Ng, J. Yip, and Y. F. Chan, "Numerical simulation of pressure therapy glove by using finite element method," *Burns*, vol. 42, no. 1, pp. 141–151, 2016.

[20] S. Shimawaki and N. Sakai, "Quasi-static deformation analysis of a human finger using a three-dimensional finite element model constructed from ct images," *Journal of Environment and Engineering*, vol. 2, no. 1, pp. 56–63, 2007.

[21] G. Harih and M. Tada, "Development of a finite element digital human hand model," in *7th International Conference on 3D Body Scanning Technologies*, 2016, pp. 208–213.

[22] D. Chamoret, M. Bodo, and S. Roth, "A first step in finite-element simulation of a grasping task," *Computer Assisted Surgery*, vol. 21, no. sup1, pp. 22–29, 2016.

[23] T.-H. Huang *et al.*, "Optimization design of thumbspica splint using finite element method," *Medical and Biological Engineering and Computing*, vol. 44, no. 12, pp. 1105–1111, 2006.

[24] L. Kuijt-Evers, T. Bosch, M. Huysmans, M. De Looze, and P. Vink, "Association between objective and subjective measurements of comfort and discomfort in hand tools," *Applied ergonomics*, vol. 38, no. 5, pp. 643–654, 2007.

[25] W. Jiang, J. Gong, H. Chen, and S.-T. Tu, "The effect of filler metal thickness on residual stress and creep for stainless-steel plate–fin structure," *International Journal of Pressure Vessels and Piping*, vol. 85, no. 8, pp. 569–574, 2008.

[26] D. Bellet, P. Lamagnere, A. Vincent, and Y. Brechet, "Nanoindentation investigation of the young's modulus of porous silicon," *Journal of Applied Physics*, vol. 80, no. 7, pp. 3772–3776, 1996.

[27] F. M. Yaul, V. Bulovic, and J. H. Lang, "A flexible underwater pressure sensor array using a conductive elastomer strain gauge," *Journal of microelectromechanical systems*, vol. 21, no. 4, pp. 897–907, 2012.

[28] T. Hou *et al.*, "Design and experiment of a universal two-fingered hand with soft fingertips based on jamming effect," *Mechanism and Machine Theory*, vol. 133, pp. 706–719, 2019.